Available online at www.sciencedirect.com
ScienceDirect
Cement and Concrete Research 38 (2008) 49–67
Cement and Concrete Research

Experimental investigation and numerical modeling of chloride penetration and calcium dissolution in saturated concrete

T. Sugiyama [a,*], W. Ritthichauy [b], Y. Tsuji [c]

[a] Hokkaido University, Graduate School of Engineering, Division of Built Environment, Sapporo, 060-8628, Japan
[b] Norconsult Civil Engineering Co., Ltd., Bangkok, 10400, Thailand
[c] Gunma University, Graduate School of Engineering, Kiryu, Gunma 376-8515, Japan

Received 9 July 2005; accepted 19 August 2007

Abstract

Chloride penetration and calcium dissolution have been investigated for a saturated concrete after exposure to a 0.5 mol/L NaCl solution for a period of up to 3150 days. Simultaneous ion transport model (SiTraM) that allows the transport of chloride and calcium ions to be simultaneously simulated in a hydrated cement system has been used to verify the experimental results.

Self-compacting concrete (SCC) with a water to cement ratio of 0.3 resulted in a limited chloride penetration depth while the calcium dissolution was also reduced within the near surface zone. Increased unit water content for normal concrete resulted in higher chloride penetration depth and larger dissolution front of $Ca(OH)_2$ regardless of having the same water to cement ratio.

It was revealed that the SiTraM can predict the profiles of chloride and calcium for self-compacting concrete. It was also found that the primary factor to control chloride penetration front and the dissolution front of $Ca(OH)_2$ was the pore structure characteristic of concrete.

Keywords: Chloride penetration; Calcium dissolution; Self-compacting concrete; Numerical calculation; Pore structure

1. Introduction

Ion transport through a hydrated cement system often becomes a primal factor to degrade concrete in an aggressive environment. Especially saturated concrete structures in seawater or exposed to ground water will be deteriorated to which degree is controlled by ion diffusion through the pore structure of the concrete. Chloride ion diffusion has become a center of attention for research on ion transport in concrete [1]. This is because of the fact that corrosion of steel bars embedded in concrete is caused by chloride ingress resulting in the most detrimental effect on the degradation of concrete structures.

In order to reduce the deterioration risk due to the corrosion of reinforcement, high performance concrete will be used such as self-compacting concrete (SCC) which is anticipated to resist against chloride ingress under harsh environmental conditions for a long period of time. In general, chloride penetration in saturated concrete will couple with the dissolution of calcium from the hydrated cement system. However, the interactive effect of chloride penetration and calcium dissolution in concrete has remained unknown. This study will focus on the dissolution of calcium in SCC as it is being used for a civil structure of extremely long term service period.

It has been known that the water to cement ratio (W/C) plays an important role on the resistance against chloride ingress in concrete. However, the effect of increased unit cement content in concrete on chloride penetration and calcium dissolution has been barely clarified. It may be beneficial because the amount of immobilized chloride ions is increased in the hydrated cement system when the amount of unit cement content is appropriately increased. In addition, it is thought that possibly the amount of dissolved calcium from the hydrated cement system is increased. However, since increased unit cement content is associated with increased unit water content possible passage for the transport of ions is increased in the concrete. In addition, from a practical point of view the risk of defects due to the construction of the concrete such as segregation may be increased.

In this present research self-compacting concrete (SCC) of a W/C of 0.3 has been exposed to 0.5 mol/L NaCl solution for

* Corresponding author. Tel./fax: +81 11 706 6178.
E-mail address: takaf@eng.hokudai.ac.jp (T. Sugiyama).

0008-8846/$ - see front matter © 2007 Elsevier Ltd. All rights reserved.
doi:10.1016/j.cemconres.2007.08.027

3150 days under controlled laboratory conditions. Chloride penetration profile and the profile of remaining calcium content are compared with those of normal concrete of a W/C of 0.55. For normal concrete, the effect of increased unit cement content and hence an increased unit water content up to 207 kg/m^3 is also studied and compared with concrete of an equal W/C but the unit water content of 178 kg/m^3. Another series of chloride penetration tests with a period of 420 days has been conducted on normal concrete of a W/C of 0.45. For these concretes, different unit water contents of 153, 163 and 173 kg/m^3 are employed, respectively. After the termination of the penetration tests, cored concrete was taken and sliced with increased depth from the exposure surface. The profile of total chloride ions in concrete was determined by the nitric acid extraction method. The remaining amount of $Ca(OH)_2$ was identified and determined by the X-ray diffraction (XRD) and the thermogravimetry/differential thermal analysis (TG/DTA), respectively.

In this paper, simultaneous ion transport model (SiTraM) has been applied to simulate both profiles of chloride and calcium. The concept of SiTraM has been already proposed by authors [2]. Therefore, this present study has been directed for the purpose of practical preference to specify the comprehensive model using three separate models so as to enhance the understanding of respective phenomenon involved in ion transport mechanism in concrete. In this sense, the time and spatial dependence of pore structure in concrete are briefly explained. In addition, selective ion diffusion phenomenon that has been reported but remained unsolved is considered in a quantitative manner. The calculation of decalcification from calcium silicate hydrate (C–S–H) is also explained. In this way, the applicability of the SiTraM to concrete subjected to chloride penetration is presented. Parameters necessary for the execution of the numerical calculation in accordance with mixture proportions and testing conditions specified in this research are determined separately.

2. Simultaneous ion transport model

A unique feature of this present simultaneous ion transport model, SiTraM is to allow both the calculations of chloride penetration profile and the profile of calcium remaining in the hydrated cement system in concrete which is exposed to chloride laden solution. It is composed of three models as shown in Fig. 1, namely Mutual ion diffusion coefficient model, Characterizing pore structure model and ion-solid interactions model. Each model is briefly discussed in the following section.

A governing equation in the SiTraM simulation is the Fick's diffusion equation. Unidirectional diffusion is considered in concrete as follows;

$$\frac{\partial C}{\partial t} = D\frac{\partial^2 C}{\partial x^2} \tag{1}$$

Where C is the concentration of ions (mol/L), D is the diffusion coefficient (cm^2/s), t and x are the time and position, respectively.

Details of the numerical description using a finite difference method for Eq. (1) are provided later in Section 5. Mobile ions

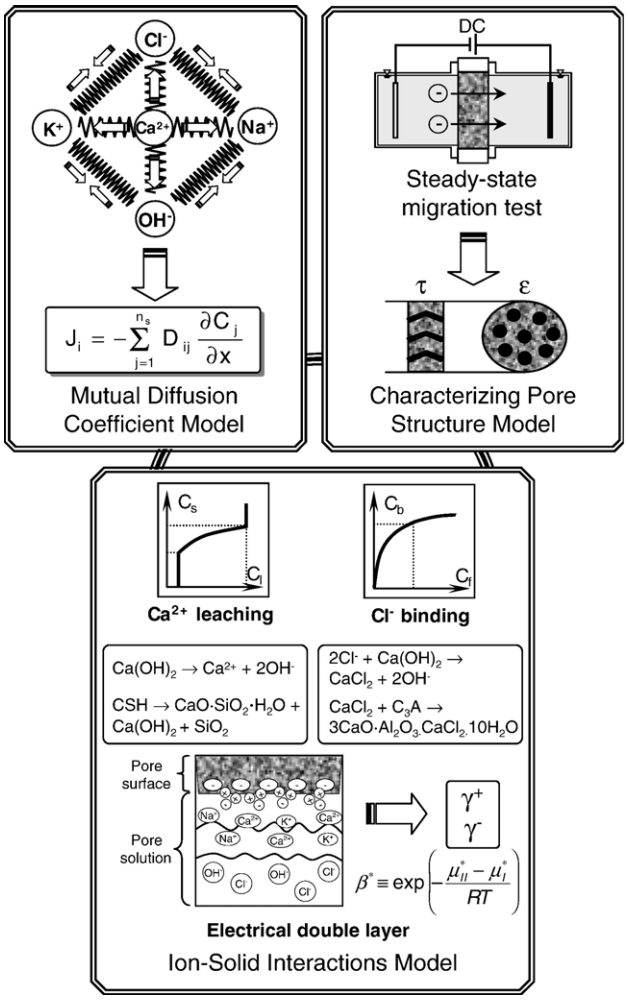

Fig. 1. Simultaneous ion transport model.

diffuse through the pore solution of concrete according to Eq. (1). Then depending on the resultant concentration in a given time and position of the pore space chemical reaction takes place instantaneously so as to follow local equilibrium between the solid and solution in the pore. Mutual ion diffusion coefficient model and Characterizing pore structure model are used so as to control the transportation of ions while ion-solid interactions model is to control the reaction parts.

2.1. Mutual ion diffusion coefficient model

2.1.1. Calculation of mutual ion diffusion coefficient

Mutual ion diffusion coefficient model allows the calculation of diffusion coefficients of various ionic species on the basis of electrochemical potential within the pore solution of concrete. Influence of coexisting different ionic species in a multicomponent solution like pore solution of concrete is quantitatively evaluated by a resultant mutual diffusion coefficient (MDC) [4,5]. MDC has been applied to ionic species present in the pore solution in a hydrated cement system [2,3]. In this paper the methodology to calculate MDC is briefly explained.

Felmy and Weare have originally developed a general form of the calculation method on MDCs of several ionic species present

in the sea water [4,5]. The MDC, i.e. D_{ij}, is the diffusion coefficient of the ith ionic species that is influenced by the concentration gradient of the jth species. This D_{ij} can be explained schematically by the diagram that is shown in the Mutual diffusion coefficient model of Fig. 1. Assuming that there are various ionic species coexisting in a solution, D_{ij} represents for each connection that binds one ionic species to another. Driving force for the diffusion of an ionic species is originated from thermodynamic force that can be considered as the gradient of electrochemical potential. Chemical potential gradient and electronic potential gradient compose of the electrochemical potential. The flux of diffusion for a given ionic species can be computed with a phenomenological transport coefficient matrix using following equation [4,6];

$$J_i = \sum_{j=1}^{n_S} l_{i,j}\left(-\frac{\partial \mu_j}{\partial x} - z_j F\frac{\partial \phi}{\partial x}\right) \tag{2}$$

Where J_i is the flux of the ith ionic species (mol/cm^2/s), $l_{i,j}$ is the phenomenological transport coefficient matrix (mol^2/cm/J/s), n_s is the number of ionic species in solution, $\partial\mu_j/\partial x$ is the chemical potential gradient of the jth species, $\partial\varphi/\partial x$ is the electronic potential gradient, z_j is the valence number of the jth ionic species, F is the Faraday's constant.

Since the electrical part is not readily measurable in electrolyte solution this part can be eliminated from Eq. (2) by taking account of the zero current constraint [4,6]. Furthermore by adopting a simplified methodology to account for wide variations in concentration gradients the phenomenological transport coefficient matrix is reduced and then Eq. (2) becomes as follows [6];

$$J_i = \frac{D_i^0 C_i}{RT}\cdot\frac{\partial \mu_i}{\partial x} + \left(\frac{z_i D_i^0 C_i}{RT\sum_{k=1}^{n_s} z_k^2 D_k^0 C_k}\sum_{k=1}^{n_s} z_k D_k^0 C_k \cdot \frac{\partial \mu_k}{\partial x}\right) \tag{3}$$

Where R is the gas constant (J/(mol·K)), T is the absolute temperature (K), D_i^0 is the tracer diffusion coefficient of the ith ionic species in dilute solution (cm^2/s).

Chemical potential gradient is converted to concentration gradient and then final set of the equation on the flux of diffusion is expressed as follows [4,6];

$$J_i = -\sum_{j=1}^{n_s} D_{ij}\frac{\partial C_j}{\partial x} \tag{4}$$

Where D_{ij} is the mutual diffusion coefficient matrix.

The formulae of this D_{ij} can be shown by the following equation [6];

$$D_{ij} = \delta_{ij} D_i^0\left(1+\frac{\partial \ln a_i}{\partial \ln C_i}\right) - \left\{\frac{z_i D_i^0 C_i}{\sum_{k=1}^{n_s} z_k^2 D_k^0 C_k} z_j D_j^0\left(1+\frac{\partial \ln a_j}{\partial \ln C_j}\right)\right\} \tag{5}$$

where δ_{ij} is designated for the Kronecker delta function which is equal to 1 if $i=j$, but equal to 0 if $i\neq j$, and a_i is the mean activity coefficient of the ith species that is assumed to be calculated according to the Debye–Huckel theory.

Fig. 2 shows the concentration dependent mutual diffusion coefficient calculated for the 1-1 type of an electrolyte of NaCl solution and KCl solution, respectively. Although available experimental results are limited for the 1-1 type electrolytes [8], calculated mutual diffusion coefficients agree well with the experiments.

2.1.2. Application to the pore solution in concrete

Mutual diffusion coefficient can be calculated by providing the values of concentration of ions present in a given calculation domain, tracer diffusion coefficient, and ion size parameter of each ionic species. Ion size parameters and tracer diffusion coefficients can be found in chemistry Ref. [7,9]. Therefore, it is necessary to provide the pore solution chemistry of concrete to calculate the MDC. Accordingly, the concentration of various ionic species present in the pore solution of concrete is determined by an electrical extraction method which has been developed by the authors for each type of cement [10,11].

It is noted that the mutual diffusion coefficient for concrete is time dependent since the composition of the pore solution chemistry changes with time. In addition, the mutual diffusion coefficient in Eq. (5) is defined as an aqueous mutual diffusion coefficient that is separately defined from an intrinsic mutual diffusion coefficient [2,3]. The intrinsic mutual diffusion coefficient is explained with relation to pore structure characteristic in the next section.

2.2. Characterizing pore structure model

2.2.1. Significance of scale factor

In order to treat the transport of ions in concrete the aqueous mutual diffusion coefficient shown in Eq. (5) is transformed to an intrinsic mutual diffusion coefficient. This needs to be done to reflect the physical nature of the pore structure in concrete. For this transformation purpose a scale factor, K was introduced.

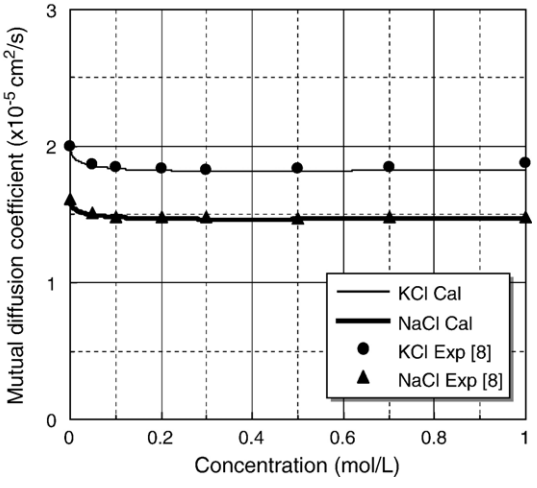

Fig. 2. Calculated concentration dependent mutual diffusion coefficients of 1-1 type electrolytes.

Then the intrinsic mutual diffusion coefficient is given by the following Eq. [2];

$$D_{ij,I}(x,t) = D_{ij}(x,t) \cdot K_{x,t} \tag{6}$$

Where K is a scale factor, subscripts x and t denote arbitrary position and time, respectively. Note that the ion transport is considered in an x-direction only.

2.2.2. Definition and determination of pore structure coefficient

Pore structure characteristic of concrete is quantitatively evaluated by the steady-state chloride migration test [12]. The concept of this model is shown as the Characterizing pore structure model in Fig. 1. In this purpose, JSCE G571-2003 is adopted for determining the effective diffusion coefficient of chloride ions. The schematic diagram of this migration test is shown in Fig. 3 [13].

From the experimental results of the migration test, the flux of chloride ions at steady-state can be achieved on concrete under investigation. Then the flux is related to the effective diffusion coefficient, i.e. D_e by the following expression [14];

$$J_i = \frac{z_i F}{RT} D_e C_i \frac{\Delta E_e}{\Delta X} \tag{7}$$

Where J_i is the flux of the ith ionic species (mol/(cm^2 s)), F is the Faraday's constant (C/mol), C_i is the concentration of the ith ionic species (mol/L), $\Delta E_e / \Delta X$ is the electrical potential gradient (V/cm).

In this way the pore structure characteristic of concrete under investigation is quantified by the following equation [12];

$$\frac{\varepsilon}{\tau^2} = \frac{D_e}{D_f} \tag{8}$$

Where ε and τ are the porosity and tortuosity of concrete under investigation, respectively, D_f is the diffusion coefficient in a given aqueous solution (cm^2/s) [12].

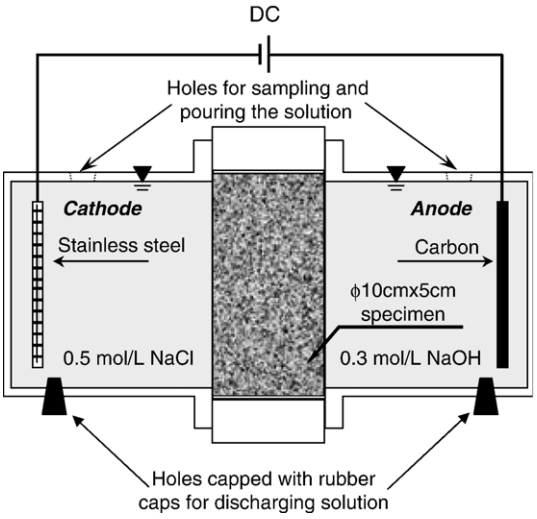

Fig. 3. Migration cell test for characterizing pore structure.

The parameter ε/τ^2 that is given in Eq. (8) was designated as the pore structure coefficient and used for the scale factor, K in this present transport model.

2.2.3. Time and depth dependent pore structure coefficient

By considering continuous cement hydration or the degree of hydration as well as the inhomogeneity of pore structure with depth, the pore structure coefficient is then defined as follows;

$$K_{x,t} = \left(\frac{\varepsilon}{\tau^2}\right)^{\text{int.}} \cdot \frac{D_e(x^0,t')}{D_e^0} \frac{D_e(x',t^0)}{D_e^0}. \tag{9}$$

Where $(\varepsilon/\tau^2)^{\text{int.}}$ is the initial pore structure coefficient, $D_e(x^0, t')/D_e^0$ and $D_e(x',t^0)/D_e{}^0$ are the normalized numbers for the effective diffusion coefficient for a given time and depth respectively, t' and x' are the normalized time (t/t^0) and depth (x/x^0), respectively.

For example, when $D_e{}^0$ is determined for concrete at 28 days and at a depth of 10 cm and used for calculating the initial pore structure coefficient, then t^0 is equal to 28 days and x^0 is equal to 10 cm. Time and depth-dependent effective diffusion coefficients need to be determined individually by steady-state migration technique for the concrete under investigation.

2.3. Ion-solid interactions model

Ion-solid interactions in saturated concrete are primarily accounted by considering the dissolution of calcium from solid $Ca(OH)_2$ and/or C–S–H, chloride binding and an effect of near pore surface for a selective ionic species. The methodology to calculate the dissolution of calcium from the hydrated cement products is briefly explained. In addition, a unique characteristic of near pore surface with regards to ion transport through the hydrated cement system is also explained.

2.3.1. Dissolution of calcium from hydrated cement system

The general concept and calculation method of the dissolution of calcium from hydrated cement system are similar to those proposed by Berner and Buil [15,16]. Although the previous research by the authors [2] has also followed their methodology there was insufficient explanation on this particular matter. Therefore the calculation of the decalcification of C–S–H is explained in this paper.

In general, the transport of calcium ions is governed by diffusion and reaction. However, local equilibrium assumption implies that the diffusion rate is very slow compared to the dissolution rate. Therefore, the rate of the system change should be controlled by diffusion [17].

The sharp drop of Poltlandite solubility is reported for the base solution of NaOH solution with increased concentration [18]. On the other hand relatively comparable solubility ranging from 0.020 to 0.028 molal $Ca(OH)_2$ is obtained in NaCl solution [18]. Furthermore chemical analysis using actual pore solution that was extracted from OPC mortar specimen showed that the concentration of calcium ions is approximately 0.02 mol/L [19]. In this way it seems that the ionic concentration of calcium ions in pore solution is uncertain and dependent on its pore solution chemistry.

It is generally understood from the experiment carried out by Berner that the concentration of calcium ions in the pore solution of cement paste remains constant during the dissolution of $Ca(OH)_2$ [15, 20]. Therefore a constant value of 0.02 mol/L for the concentration of calcium ions in pore solution can be assumed so as not to underestimate its dissolution mechanism as suggested by Saito et al. [21]. The effect of adopting this specific concentration of calcium ions can be minimized in this present model by the inclusion of pore surface effect which is explained later in Section 2.3.5 in this paper.

Immediately after the reduction of the concentration of calcium ions in pore solution, instantaneous dissolution will supply calcium from the solid calcium (initially in $Ca(OH)_2$) so as to compensate for the amount of calcium ions that diffuses out. Consequently, the concentration of calcium ions in the pore solution will be again increased to its initial concentration, i.e. 0.02 mol/L. These repeatedly reversible reactions will always be able to maintain the concentration of calcium ions unless the $Ca(OH)_2$ in the section considered is depleted.

2.3.2. Decalcification of C–S–H from hydrated cement system

After the depletion of solid $Ca(OH)_2$, the decalcification of C–S–H starts in the considered section. At this point the concentration of calcium ions in pore solution will not be maintained at 0.02 mol/L. In contrast, the concentration of calcium in solid structure as C–S–H can be in a chemical potential equilibrium with that in the pore solution.

A schematic diagram for the calculation of C–S–H decalcification that is adopted in this present model is shown in Fig. 4. The *y*-axis in this figure is the concentration of calcium in the solid phase where a constant silica content is assumed. The *x*-axis is that of calcium ions in pore solution in the same unit of mol so that the amount of calcium for reduction and compensation can be easily understood.

The nonlinear relation of a liquid–solid equilibrium which is shown in the curved portion B–C in Fig. 4 is defined by Buil et al. [16].

At a particular time and position, after depletion of $Ca(OH)_2$ (as designated by dotted line A–B), the concentration of calcium ions (C_1) in pore solution is assumed to be in equilibrium with the concentration of calcium in C–S–H (CSH_1). Due to a concentration gradient which results in the reduction of its concentration (−*fdt*, in Fig. 4), C_1 is reduced to C_2. At this point which is designated by a star mark in the same figure, the relation of calcium concentration in solid phase and that in pore solution is on the equilibrium curve line. For this reason, the chemical equilibrium system will adjust the disturbed equilibrium by liberating some calcium from C–S–H. Assuming that the released amount of calcium from the solid phase is equal to ΔX, hence the amount of calcium ions in aqueous phase must also be increased by this ΔX. Eventually, the remaining amount of calcium ions in pore solution and that in solid phase is equal to C_3 and CSH_3, respectively.

If the concentration of calcium in solid phase is decreased until point C of Fig. 4, the decalcification of C–S–H will be instantaneous and similar to the dissolution of $Ca(OH)_2$ as shown by the sharp linear portion C–D in the figure. At this part, the concentration of calcium ions in pore solution will be a constant value of 0.0015 mol/L [15,20].

2.3.3. Chloride binding isotherm in concrete

Penetrating chloride ions into the pore solution of concrete is bound by the C_3A phase in the form of the Friedel's salt. In addition, ion exchange and sorption onto the C–S–H phase are considered as other immobilizing mechanisms for the diffusion of chloride ions. However the binding phenomena for chloride ions with hydrated cement system will be more complex and hardly quantified to account for each mechanisms involved. Therefore from relatively macroscopic points of view the amount of the bound chloride is calculated as a function of the concentration of free chloride ions as shown in Eq. (10) [22];

$$C_b = e^{\alpha_{OH}\left(1-\frac{[OH]}{[OH]_{ini}}\right)} \cdot e^{\frac{E_b}{R}\left(\frac{1}{T}-\frac{1}{T_0}\right)} \cdot W_{gel} \cdot \frac{\alpha}{1000} C_{ff}^{\beta} \tag{10}$$

Where α_{OH} is the constant for hydroxide-dependent effect, [OH] is the concentration of OH^- (mol/L), $[OH]_{ini}$ is the initial concentration of OH^- (mol/L), E_b is the activation energy for

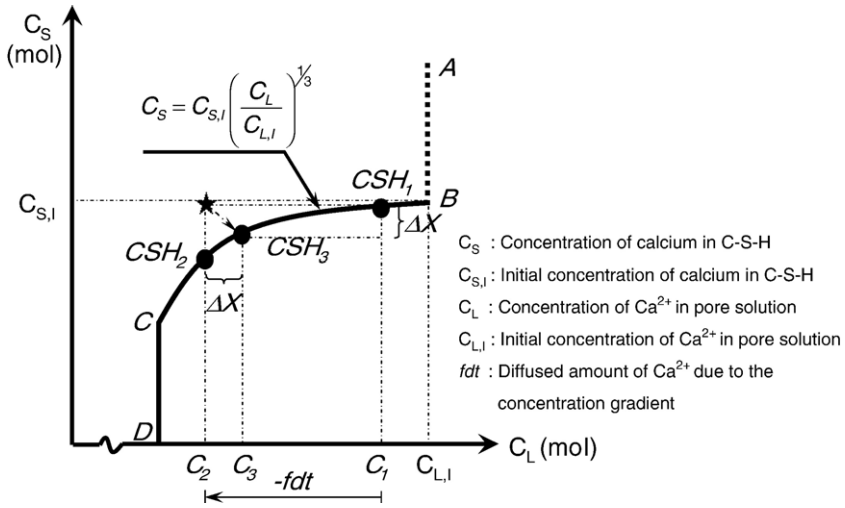

Fig. 4. Method of the calculation of C–S–H decalcification.

chloride binding (40,000 J/mol), T_0 is the absolute temperature at which the binding isotherm is obtained (293 K), C_{ff} is the concentration of free chloride ions (kg/m^3-solution), W_{gel} is the amount of hydration gel (kg$_{gel}$/m^3-material).

The empirical parameters for chloride binding isotherm shown in Eq. (10), i.e. α and β were determined by the experimental method proposed by Tang and Nilsson [23]. These parameters are controlled by the type of cement.

2.3.4. Selective ion diffusion near pore surface

Ushiyama and Goto have reported the results of the diffusion cell test that anions were more diffusible than cations through hardened cement paste showing the order of the diffusion coefficients for each ionic species as follows, $Cl^- > K^+ > Na^+ > Li^+$ [24]. In addition, Goto and Roy have reported higher activation energy for sodium ions than that of chloride ions implying an effect of the pore surface charge [25]. The authors of this paper have also confirmed by both migration cell and diffusion cell tests that the diffusion coefficients were in ordered as $Cl^- > K^+ > Na^+$ which was the same as Ushiyama's findings [26]. In this way it is appropriate to consider for a hydrated cement system to have a function of selective ion diffusion. Since the mutual diffusion coefficient model is responsible for an ion–ion interaction within the pore solution, selective ion diffusion phenomenon should be considered separately as a near pore surface effect in this present model.

Quantitative evaluation of the near pore surface effect still cannot be performed precisely. However, the different diffusion kinetics of sodium ions and potassium ions in a hydrated cement system will be due to the resultant different concentrations in the pore solution. Shigeru et al. has pointed out that the concentration of chloride ions was higher than that of paired sodium ions in cement paste specimen removed after the termination of the diffusion cell test [27]. This was explained by the different distribution coefficient that was defined by the difference in the concentration of ions in between the cement paste and the NaCl solution used for the diffusion cell test. Distribution coefficient for a solute between two dilute solutions is generally expressed as follows [28];

$$\beta^* \equiv \frac{c_{II}}{c_I} = \exp\left(-\frac{\mu^*_{II} - \mu^*_I}{RT}\right) \tag{11}$$

Where β^* is the distribution coefficient, c_I/c_{II} is the ratio of concentrations of solutes between solution I and solution II which are in contact with each other, and μ is the idealized chemical potential of the solute in each solution.

In order to apply Eq. (11) to the present ion-solid interactions model, an apparent specific distribution coefficient for sodium ions and potassium ions is defined so as to reflect their relative diffusion kinetics to that of chloride ions.

Apparent specific distribution coefficient, γ is defined and calculated by the following formula;

$$\gamma^i = \frac{D^*_{e,i}}{D^*_{e,Cl}} \tag{12}$$

Where γ^i is the apparent specific distribution coefficient as dimensionless parameter for the ith ionic species, $D^*_{e,i}$ is the standardized effective diffusion coefficient of alkali ions (cm^2/s), $D^*_{e,Cl-}$ is the standardized effective diffusion coefficient of chloride ions (cm^2/s).

In order to calculate the apparent specific distribution coefficient used in Eq. (12) another series of the steady-state chloride migration tests were conducted. Standardized effective diffusion coefficients are then determined for alkali ions as well as chloride ions. Unique feature in calculating standardized effective diffusion coefficients is to use the concentration of each ionic species that is present within concrete specimen after the termination of the steady-state migration test. Relative concentration difference in alkali and chloride ions within the concrete specimen is reflected to standardized effective diffusion coefficients. Details and migration test results are given in Section 5.1.4.

Since it is assumed that the pore surface effect rarely has an influence on the transport of anions, this γ is equal to 1.0 for all anions in the present model.

2.3.5. Pore surface effect on the diffusion of calcium ion

Chatterji and Kawamura have reported on the presence of the Gouy–Chapman layer, in which its estimated positive ion concentration, especially that of calcium ions is much higher than that of the bulk pore solution [29]. This higher concentration of calcium ions near the pore surface seems to be a contrast to the fact on common knowledge on the concentration of calcium ions in the pore solution of hydrated cement system i.e. 0.02 mol/L. Nevertheless this evidence supports experimental results that normally exhibit larger amounts of calcium ions being diffused into a leachant as compared with those of sodium ions and potassium ions in a leaching test. This fact is hardly explained by the concentration gradient of calcium ions as the driving force that is much less than those of the alkali ions [30]. Therefore, in this present ion-solid interactions model, the related pore surface effect on the diffusion of calcium ions was represented by the apparent specific distribution coefficient, γ^i. In other words, it is assumed that the effective chemical potential for calcium ions to diffuse through the pore structure is apparently larger than that induced by the concentration of a constant 0.02 mol/L. Accordingly the diffusion of calcium ions can be treated in a similar manner to the diffusion of sodium ions and potassium ions.

2.4. Alteration of pore structure characteristic due to ion-solid interactions

Besides the time and position dependence of pore structure characteristic due to cement hydration and inhomogeneity, it will be also altered by dissolution and/or precipitation phenomenon as a result of ion-solid interactions. At this present, there is no certainty about the change of the tortuosity due to the dissolution and precipitation. Therefore it is assumed that the porosity is either increased by dissolution or decreased by precipitation in the present model. Then the change of porosity is expressed by the following equation;

$$\varepsilon_{x,t} = \varepsilon^{Ini} + \Delta\varepsilon^{Dsl}_{x,t} - \Delta\varepsilon^{Pcp}_{x,t} \tag{13}$$

Where ε^{Ini} is the initial porosity, $\Delta\varepsilon^{Dsl}_{x,t}$ is the increased porosity due to the dissolution of solid calcium, $\Delta\varepsilon^{Pcp}_{x,t}$ is the

Table 1
Physical properties and chemical compositions of cement binder

Physical properties/chemical composition		Type of cement binder	
		OPC	LHC
Physical properties	Specific gravity	3.16	3.22
	Specific surface (cm^2/g)	3310	3430
Chemical composition	CaO (%)	64.3	63.1
	SiO_2 (%)	20.9	26.2
	Al_2O_3 (%)	5.24	2.62
	Fe_2O_3 (%)	2.88	2.51
	SO_3 (%)	2.05	2.25
	Na_2O (%)	0.27	0.20
	K_2O (%)	0.40	0.36
	MgO (%)	1.33	1.81

decreased porosity due to the precipitation of the Friedel's salt, subscripts x, and t denote arbitrary position and time, respectively.

The change of porosity due to the dissolution and precipitation needs to be reflected in Eq. (9) by multiplying the variable, $\varepsilon_{x,t}/\varepsilon^{\mathrm{Ini}}$.

2.4.1. Effect of solid calcium leaching on the pore structure

Depending on the amount of dissolved calcium from the hydrated cement system pore space can be increased. The expression for this increase is shown in Eq. (14) [16];

$$\Delta\varepsilon_{x,t}^{\mathrm{Dsl}} = \rho_c \cdot \frac{MW_{\mathrm{CH}}}{d_{\mathrm{CH}}} \cdot \left(\mathrm{SC}^{\mathrm{Ini}} - \mathrm{SC}_{x,t}\right) \tag{14}$$

$$\rho_c = 1 - \frac{1}{d_C(W/C)+1} \tag{15}$$

Where ρ_c is the volume density of the cement paste, d_C is the density of cement (g/cm^3), W/C is the water to cement ratio, $\mathrm{MW_{CH}}$ is the molecular weight of $Ca(OH)_2$ (g/mol), d_{CH} is the density of $Ca(OH)_2$ (g/l), $\mathrm{SC}^{\mathrm{ini}}$ is the initial solid calcium concentration (mol/L-solid), and $\mathrm{SC}_{x,t}$ is the solid calcium concentration at a particular position and time (mol/L-solid), subscripts x and t denote the position x at time t, respectively.

According to Eq. (14), it is assumed that the dissolution of $Ca(OH)_2$ has the same consequence on the transport properties of the hydrated cement system as the decalcification of C–S–H. Therefore, the increased porosity is calculated by the reduction of total calcium which is the summation of that in $Ca(OH)_2$ and C–S–H.

2.4.2. Effect of chloride binding on the pore structure

It is assumed that the amount of bound chloride which is calculated by Eq. (10) can be used as the solid volume increase in pore structure. By knowing the density and molecular weight of the Friedel's salt (density = 1.892 g/cm^3, molar volume = 296.66 cm^3/mol [31], one can convert an amount of bound chloride into a solid volume. As a result, the reduction of porosity is calculated by the following equation;

$$\Delta\varepsilon_{x,t}^{\mathrm{Pcp}} = \frac{C_{x,t}^{b} \cdot \mathrm{MV_{FS}}}{1000 \cdot \mathrm{MW_{FS}}} \tag{16}$$

Where $\Delta_{\varepsilon x,t}^{\mathrm{Pcp}}$ is the decreased porosity due to the precipitation of the Friedel's salt at a particular time and position, $\mathrm{MV_{FS}}$ is the molar volume of the Friedel's salt (296.66 cm^3/mol), $\mathrm{MW_{FS}}$ is the molar weight of the Friedel's salt (561 g/mol).

3. Experimental works

3.1. Material properties and mix proportions of concrete

The types of cement used in this research were ordinary Portland cement (OPC) and low heat Portland cement (LHC). The physical properties and chemical compositions are shown in Table 1. River sand was used as the fine aggregate while the crushed stone was used as the coarse aggregate. The specific gravity, water absorption and the fineness modulus of fine and coarse aggregates are shown in Table 2.

Mix proportions and compressive strength of concrete tested in Series 1 and Series 2 are shown in Table 3. SCC specimen which is referred as a self-compacting concrete was mixed with LHC binder with a water to cement ratio of 0.3. Polycarboxylate-type superplasticizer was used for the SCC specimen. Specimens of S5, S18, and S18T are referred as normal concrete that were mixed with OPC with a constant W/C of 0.55. The number of either "5" or "18" that was shown in the designation of each mix proportion is expressed for the target slump values. For these normal concretes it was intended that the effect of increased unit cement content and hence increased unit water content on the chloride penetration and calcium dissolution was investigated. Since no chemical admixtures were used for the normal concrete the unit water content of S18 and S18T specimens was increased by 29 kg/m^3 larger than that of S5 specimen.

The compressive strength at 28 days of SCC specimen is higher than those of normal concretes tested in Series 1. It is obvious that the bleeding of SCC hardly occurred. In addition

Table 2
Physical properties of fine/coarse aggregate

Properties	Series-1		Series-2	
	Fine aggregate (River sand)	Coarse aggregate[a]	Fine aggregate (River sand)	Coarse aggregate[a]
Specific gravity (dry)	2.61	2.65	2.63	2.86
Water absorption (%)	2.45	1.24	1.50	0.73
Fineness modulus	2.50	6.53	2.49	6.48

[a] Maximum size was 20 mm.

Table 3
Mix proportions of concretes

Specimens	W/C	Slump (cm)	s/a	Air (%)	Unit weight of material (kg/m^3)				σ [a](N/mm^2)	Bleeding amount (cm^3/cm^2)
					W	*C*	*S*	*G*		
SCC [b]	30	64.0 [c]	52	2.0	175	582	851	790	71.0	0
S5	55	5	44	2±0.5	178	324	803	1035	49.2	0.05
S18		18			207	376	751	968	43.6	0.17
S18T										
CW153	45	8	48	5.5	153	340	873	1044	61.4	
CW163			47	4.3	163	362	834	1038	59.8	
CW173			43	5.0	173	384	744	1088	56.9	

[a] 28 days compressive strength.
[b] Low heat Portland cement is used as cement binder, Polycarboxylate-type superplasticizer is used by 1.58% to cement content.
[c] Slump flow, V-funnel test: 12.7 s.

increased unit water content for normal concrete resulted in larger amount of bleeding for S18 and S18T while S5 also exhibited some bleeding as shown in Table 3. It was considered that the bleeding would have some effects on chloride penetration and calcium dissolution. For S18T specimen, tamping operation was carried out on the top surface placed by the fresh concrete after the termination of the bleeding. Tamping is normally implemented to avoid subsidence cracks for a reinforced concrete member.

For CW153, CW163 and CW173 in Series 2 the water to cement ratio was constant at 0.45 while the unit water content ranged from 153 to 173 kg/m^3. Accordingly, the effect of the increased unit water content and hence the amount of cement paste on chloride penetration and calcium dissolution was also studied in Series 2 as well. OPC was used for every concrete in Series 2.

3.2. Chloride penetration test for concrete

Concretes were cast in the 15×15×20 cm^3 and 10×40×10 cm^3 rectangular steel moulds for Series 1 and Series 2, respectively. After 24 hours of the placement, concretes were demoulded and cured in a saturated $Ca(OH)_2$ solution for 3 months in a temperature-humidity controlled room (23±2 °C, 60±5% RH.).

After curing, concretes were permitted to be dried in a laboratory room for a few days. Then an epoxy adhesive was carefully coated on all surfaces except the top surface which was placed by fresh concrete.

Schematic diagrams of chloride penetration test of both concretes tested in Series 1 and Series 2 are shown in Fig. 5. The top surface of each concrete specimen was exposed to NaCl solution for a period of 3150 days for Series 1 and 420 days for Series 2, respectively.

The volume of NaCl solution with a concentration of 0.5 mol/L was approximately 1.5 L over the surface area of 225 cm^2 and 400 cm^2 for Series 1 and Series 2, respectively. The NaCl solution was periodically renewed and the penetration test was continued in a temperature-humidity controlled room(23±2 °C, 60±5% RH.).

After the completion of the chloride penetration tests, a ∅10 cm×20 cm core was taken out from each rectangular specimen tested in Series 1 as shown in Fig. 5. Two cores of ∅5 cm×10 cm were taken from each rectangular specimen tested in Series 2. Then, the slices of 0.7 to 1.0 cm in thickness were cut from the top layer to the inner portion by diamond saw.

3.3. Preparation of the powdered material for chemical analysis (nitric acid extraction, XRD and TG/DTA methods)

The nitric acid extraction method was employed for the determination of total chloride content in concrete (JCI-SC4). In addition, the X-ray diffraction (XRD) and the thermogravimetry/differential thermal analysis (TG/DTA) were carried out primarily for the identification of calcium hydroxide and the Friedel's salt.

Sliced thin disks with a thickness of 0.7 to 1.0 cm were powdered using ceramic mortar and pestle. After all powder were able to pass through the 90 μm of the sieve, these samples were kept in vacuumed desiccators for 24 hours. Then, the powder (mass=2 g) was centrifuged within a heavy liquid which was the composite solution of the bromoform and the ethanol (ratio 85 ml: 10 ml, the target specific gravity=2.325). The centrifugation speed was set to 3500 rpm for 10 min, and it was performed repeatedly until there was a clear separation in the solution of the floatable and sinkable substances. These substances were extracted from the solution and left to dry in vacuumed desiccator for 24 hours. Then, the XRD and TG/DTA analysis were conducted to identify and estimate the amount of $Ca(OH)_2$ in the powdered sample.

4. Experimental results for chloride penetration and calcium dissolution

4.1. Identification of calcium hydroxide and Friedel's salt by XRD

Results of the XRD pattern are shown in Fig. 6(a) to Fig. 6(d) for each position in concrete specimens of SCC, S5, S18, and S18T, respectively. These XRD patterns confirm the depth at which the calcium hydroxide crystal and a complex salt as a result of chloride binding, e.g. the Friedel's salt are present in each sliced concrete. The number shown in the right indicates the depth from the exposure surface that is represented as the middle of each slice cut from the core.

The XRD patterns for every slice of SCC specimen in Fig. 6(a) exhibit that there are remaining $Ca(OH)_2$ in every slice, even in the first slice of this specimen after 3150 days' exposure to

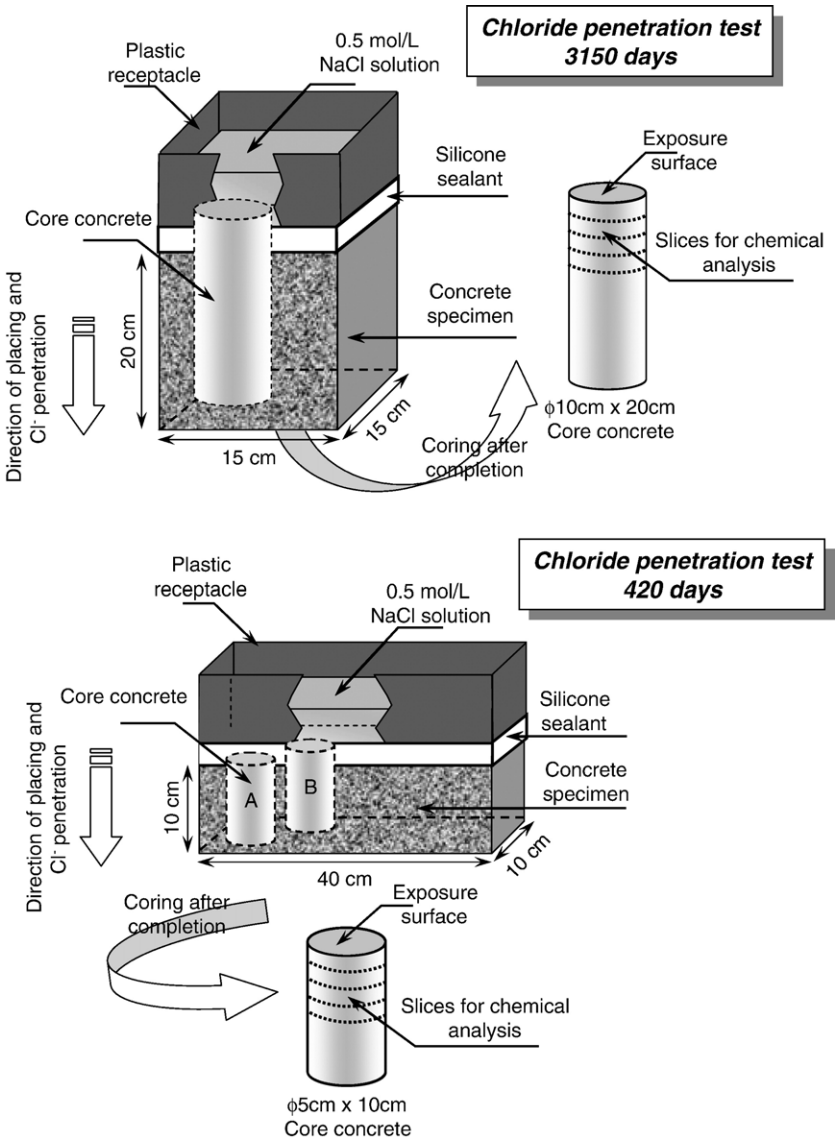

Fig. 5. Schematic diagram of chloride penetration test and coring for chemical analysis of concrete.

chloride solution. In addition, it is clearly shown by this figure that the existence of the Friedel's salt can be confirmed only in the first and the second slice. Therefore, significantly lower chloride penetration depth is apparent for the SCC specimen.

From Fig. 6(c), the existence of the $Ca(OH)_2$ crystal is confirmed for the depth equal to or larger than 2.54 cm from the exposure surface on concrete specimen of S18.

On the other hand, no $Ca(OH)_2$ can be confirmed in the first and second slices. Therefore it can be said that the dissolution front of $Ca(OH)_2$ would reach at 1.45–2.54 cm from the surface of this specimen. This XRD pattern also exhibits the existence of Friedel's salt from the first slice until the fifth slice (5.66 cm). The formation of the Friedel's salt in this XRD pattern is closely related to the depth of penetrating chloride ions from the exposure solution.

Table 4 summarizes the depth of the depletion of the $Ca(OH)_2$ crystal and the presence of the Friedel's salt for each concrete specimen. SCC exhibits no depletion of $Ca(OH)_2$. S5 shows lower depth for the depletion and the presence of the Friedel's salt as compared to those of S18 and S18T specimens despite the same water to cement ratio.

4.2. Confirmation of calcium hydroxide and the Friedel's salt by DTA

DTA curves are shown in Fig. 7(a) to Fig. 7(d) for each slice cut from cored concrete of SCC, S5, S18, and S18T, respectively. This analytical method allows for the amount of $Ca(OH)_2$ to be estimated. The estimation of the amount of $Ca(OH)_2$ with a DTA curve was followed by Suzuki's method [32]. For this purpose the appearance of the downward curve at temperature range of 420–450 °C from DTA curves are used. Moreover, the existence of the Friedel's salt can also be confirmed by these DTA curves at a temperature nearby 350 °C. However since it is difficult to

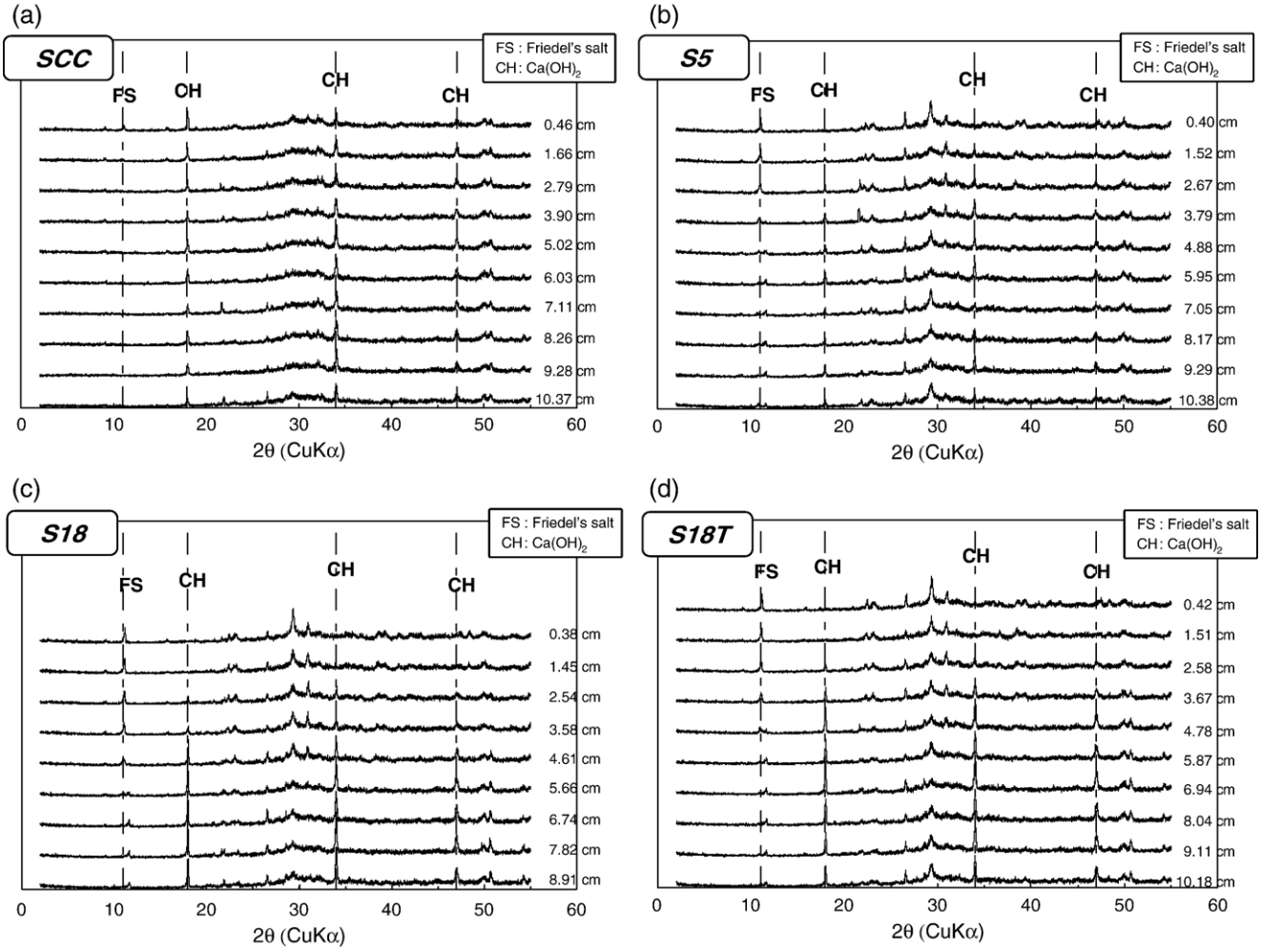

Fig. 6. Results of XRD patterns for concrete specimens tested in Series 1.

calculate the amount of this compound, only the amount of $Ca(OH)_2$ was determined from DTA curves.

DTA curves for SCC specimen show remarkable peak at the temperature range of 420–450 °C for every slice. It implies that the $Ca(OH)_2$ still remains in every slice of SCC. In contrast, the first slice of S5, and the first and second slices of S18 and S18T specimens show no peak at this temperature range indicating the depletion of $Ca(OH)_2$ in these slices. This agrees with the corresponding XRD pattern that $Ca(OH)_2$ crystal is hardly identified at the same depth for these specimens.

In this way the depletion of the $Ca(OH)_2$ and the presence of the Friedel's salt which were identified by XRD pattern can be shown consistent with the results by the TG/DTA analysis.

Table 4
Position of indication by XRD patterns for the depletion of $Ca(OH)_2$ and the presence of Friedel's salt from chloride penetration test

Specimens	Depletion of $Ca(OH)_2$		Presence of Friedel's salt	
	Slice no.[a]	Position (cm)[b]	Slice no.[c]	Position (cm)[b]
SCC	–	–	1~3	0~2.79
S5	1	0~0.40	1~4	0~3.79
S18	1, 2	0~1.45	1~5	0~4.61
S18T	1, 2	0~1.51	1~5	0~4.78

[a] Shows for the slice that cannot be indicated.
[b] Measured from the exposure surface to the center of the last slice.
[c] Shows for the slices that can be indicated.

5. Comparison with simultaneous ion transport model

5.1. Determination of input parameters

Input parameters to characterize each concrete and testing conditions employed in this research have to be specified to execute the numerical calculation.

5.1.1. Initial concentration of ions present in pore solution

Mutual diffusion coefficients were calculated for calcium, sodium, potassium, sulfate, chloride and hydroxide ions. Initial concentrations of sodium and potassium ions were determined using an electrochemical removal method for the binders of OPC and LHC [11]. The concentration of sulfate ions was calculated with the Taylor model [33]. By appointing the calcium ions

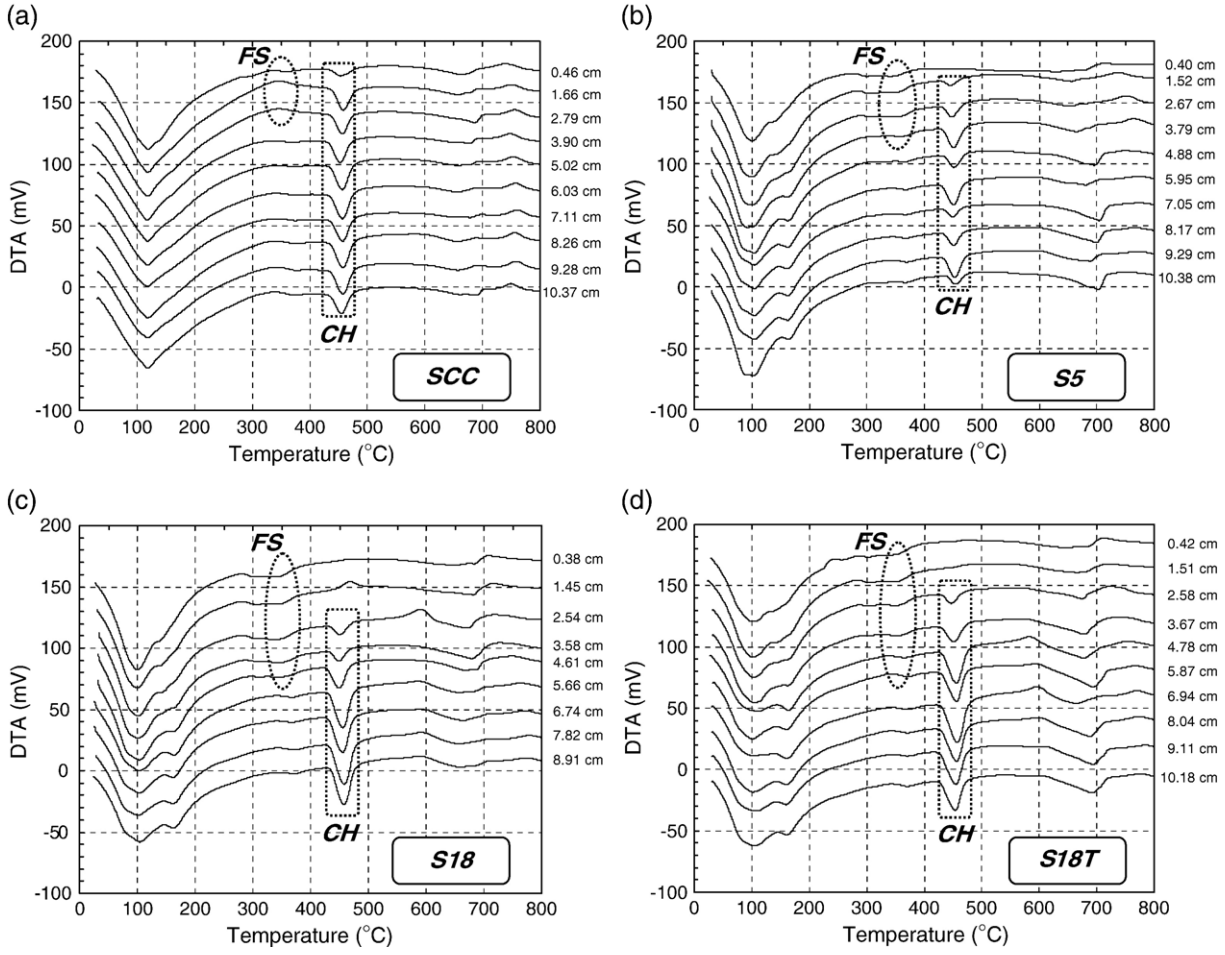

Fig. 7. Results of DTA curves for concrete specimens tested in Series 1.

concentration equal to 0.02 mol/L the electroneutrality constraint permitted for the concentration of hydroxide ions to be calculated.

Initial concentration of each ionic species present in concrete tested in Series 1 is provided in Table 5. It was assumed that the initial concentration of each ionic species present in the pore solution was equivalent as long as the same cement type was used in this research. In Table 6 calculated mutual diffusion coefficients for each ionic species initially present in the pore solution of concrete are given.

5.1.2. *Effect of the degree of hydration on pore structure coefficient*

The changes in the effective diffusion coefficient of chloride ions by the steady-state migration test was empirically

Table 5
Input parameters for calculation by the simultaneous ion transport model (Series 1)

			SCC	S5	S18	S18T
Initial pore solution concentration	$[Ca^{2+}]$ (mol/L)		0.02		0.02	
	$[Na^{+}]$ (mol/L)		0.130		0.135	
	$[K^{+}]$ (mol/L)		0.087		0.104	
	$[SO_4^{2-}]$ (mol/L)		0.003		0.003	
	$[OH^{-}]$ (mol/L)		0.252		0.273	
Pore structure characteristic	Initial porosity (ε^{ini})		0.12	0.16	0.16	0.16
	Initial pore structure coefficient ε/τ^2		1.60×10^{-3}	4.50×10^{-3}	6.34×10^{-3}	$6.34^{\times}10^{-3}$
Ions-solid interactions	Solid calcium	Initial $Ca(OH)_2$ ($\times10^3$ mol/m^3)	0.517	0.226	0.535	0.530
		Initial C–S–H ($\times10^3$ mol/m^3)	2.136	1.204	1.393	1.393
	Chloride binding isotherm	W_{gel} (kg/m^3–concrete)	737	423	494	494
		α	2.53		3.15	
		β	0.61		0.54	
	Apparent specific distribution coefficient	γ^{K}	0.75		0.77	
		γ^{Na}	0.34		0.37	
		γ^{Ca}	4.8		7.1	

Table 6
Mutual diffusion coefficients for initial concentration of OPC-based specimens (x 10^{-5} cm^2/s)

		j				
	i	Ca^{2+}	Na^+	K^+	SO_4^{2-}	OH^-
$[D_{ij}]$	Ca^{2+}	0.751	−0.021	−0.031	0.036	0.078
	Na^+	−0.147	1.146	−0.177	0.202	0.444
	K^+	−0.167	−0.136	1.668	0.229	0.504
	SO_4^{2-}	0.005	0.004	0.006	1.508	−0.016
	OH^-	1.176	0.959	1.416	−1.614	1.136

expressed as a function of time using following equation [34];

$$D_e = k \cdot t^n \tag{17}$$

Where t is the elapse time (day), k and n = empirical constants.

With a constant temperature the degree of hydration reflects the time dependent change of the pore structure coefficient for each concrete.

Empirical constants in Eq. (17) were determined with effective diffusion coefficients which were obtained using standard cylinder specimens of similar mix proportions at different curing periods. Fig. 8 shows the time dependent change of the normalized number of the effective diffusion coefficients for each concrete in Series 1. T^0 was equal to the curing period of 28 days and then $D_e{}^0$ was the effective diffusion coefficient obtained at the 28 days. Migration test results to determine $D_e{}^0$ for each mix proportion are given in Fig. 9 in which cumulative chloride ion content measured at the anode compartment is plotted with elapsed time. In this way, the relationship on the T/T^0 and $D_e/D_e{}^0$ which is given in Fig. 8 is obtained and used as the related input data.

5.1.3. Inhomogeneity of pore structure in depth

Since the direction of chloride penetration was parallel to the direction of the placing concrete then the depth-dependent effect on the pore structure coefficient was expected to emerge.

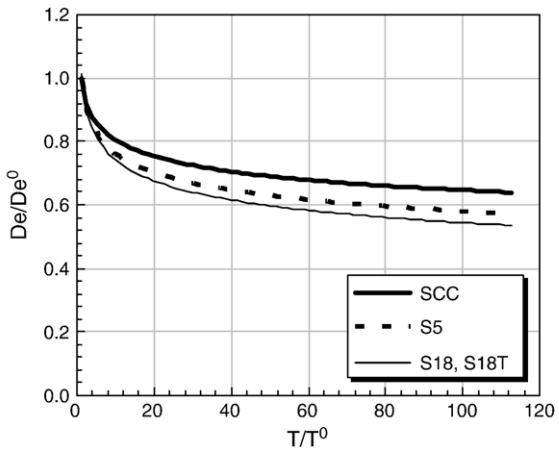

Fig. 8. Normalized time-dependent effective diffusion coefficients of concretes in Series 1.

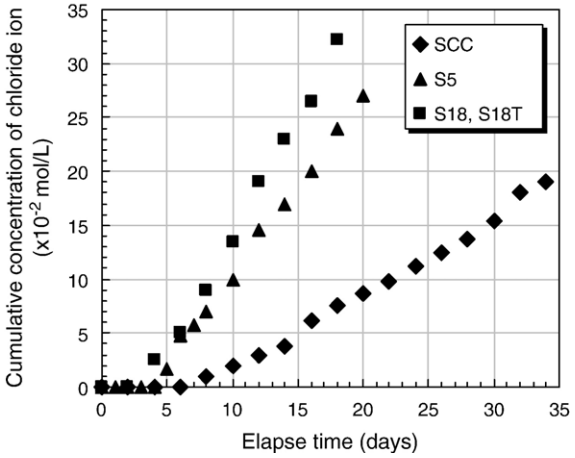

Fig. 9. Results of the steady-state migration tests of concretes in Series 1.

For the purpose of investigating the depth-dependent effect, two effective diffusion coefficients at two different locations of the upper and lower portions of a single cylinder specimen were obtained for this study. Then it was assumed to be given by the following linear relationship;

$$D_e = m \cdot x + c \tag{18}$$

Where x is the position in one dimensional direction of concrete (cm), m and c are the empirical constants.

It was found that the effective diffusion coefficient of chloride ions tends to be higher for the upper portion than that of lower portion for S18, S18T and S5. On the contrary, SCC exhibited constant effective diffusion coefficient along the depth. Therefore, the SCC was considered to avoid the depth dependent effect. Fig. 10 shows the depth dependent change of the normalized effective diffusion coefficient for each concrete in Series 1. X^0 is equal to 10 cm from the top and then $D_e{}^0$ is the effective diffusion coefficient obtained from this corresponding location. The relationship on the X/X^0 and $D_e/D_e{}^0$ given in Fig. 10 is used as the related input data.

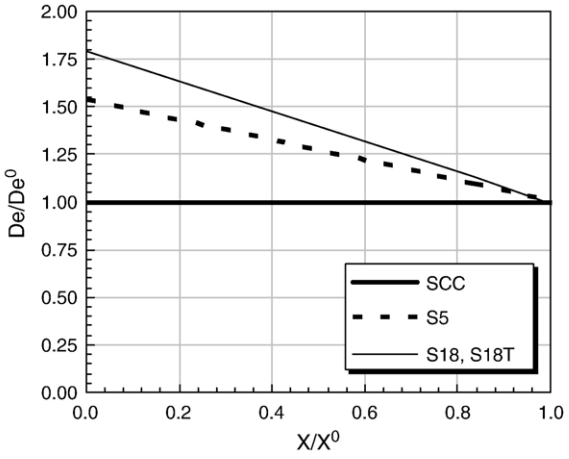

Fig. 10. Normalized position-dependent effective diffusion coefficients of concretes in Series 1.

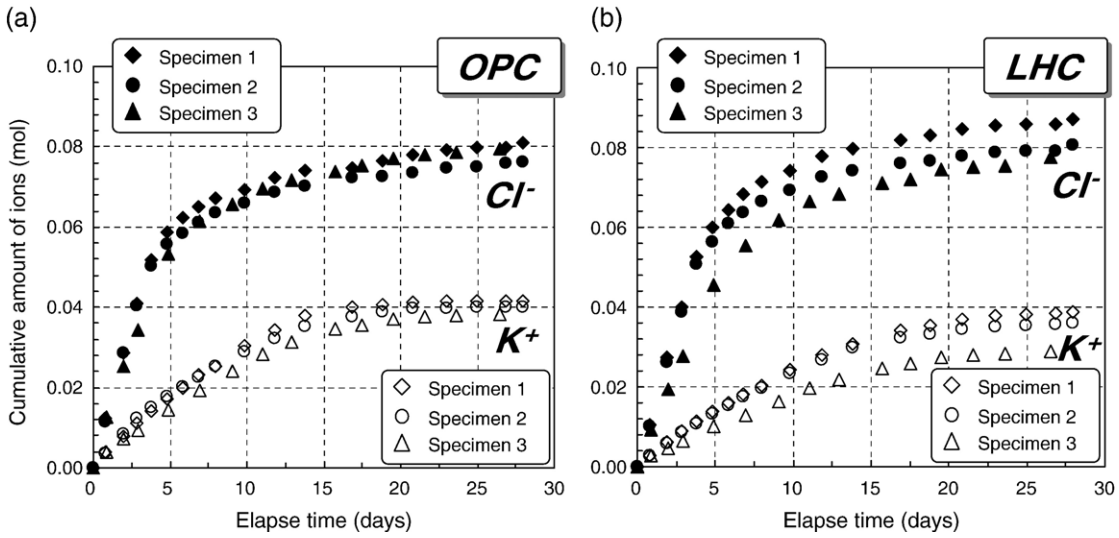

Fig. 11. Results of the extraction technique for Cl^- and K^+ of OPC and LHC based specimens.

5.1.4. Determination of apparent specific distribution coefficient, γ

Concentrations of sodium, potassium and chloride ions within concrete taken after migration tests were determined by an electrical extraction technique [10,11]. Ordinary steady-state migration test was at first conducted using the migration cell shown in Fig. 3 with the same molar concentration (0.3 mol/L) in either NaCl–KOH solutions or KCl–NaOH solutions as the cathode-anode solution combination, respectively. Next, the extraction technique with a $Ca(OH)_2$–$Ca(OH)_2$ solution combination was employed on the same concrete tested under the ordinary steady-state migration tests. Fig. 11 provides the results of the extraction technique for 3 specimens for each type of cement, showing higher concentration of chloride ions extracted as compared with that of potassium ions with elapsed time. Chloride ions concentration was measured at the anode compartment while potassium ions concentration was measured at the cathode. Higher concentration of chloride ions means that the concentration of chloride ions present in the concrete was higher than that of potassium ions after the first ordinary migration test with the NaCl–KOH solution combination of the same molar concentration. Similarly, chloride ions concentration was higher than that of sodium ions after the ordinary migration test with the KCl–NaOH solution combination. On the basis of these results, real concentration of each ionic species present within the concrete under investigation was determined. Subsequently, standardized effective diffusion coefficients were calculated for sodium, potassium and chloride ions. Apparent specific distribution coefficients as defined in Eq. (12) for sodium and potassium ions are provided in Table 5.

For the purpose of the determination of an apparent specific distribution coefficient for calcium ions, its diffusion kinetics was evaluated by a diffusion leaching experiment. From the leaching test, the amount of the leaching calcium ions was measured in the

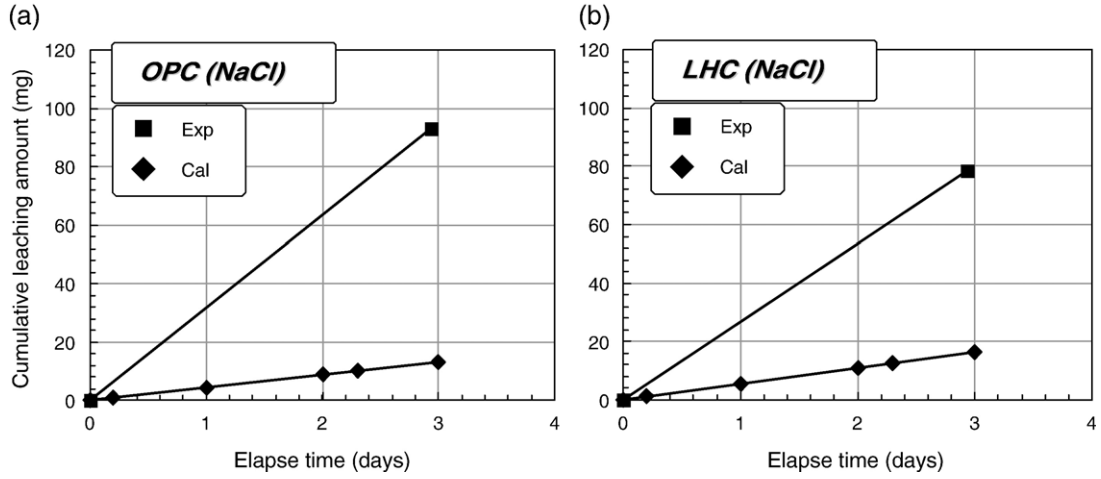

Fig. 12. Leaching amount of Ca^{2+} from the diffusion leaching test and the calculation on OPC and LHC based specimens.

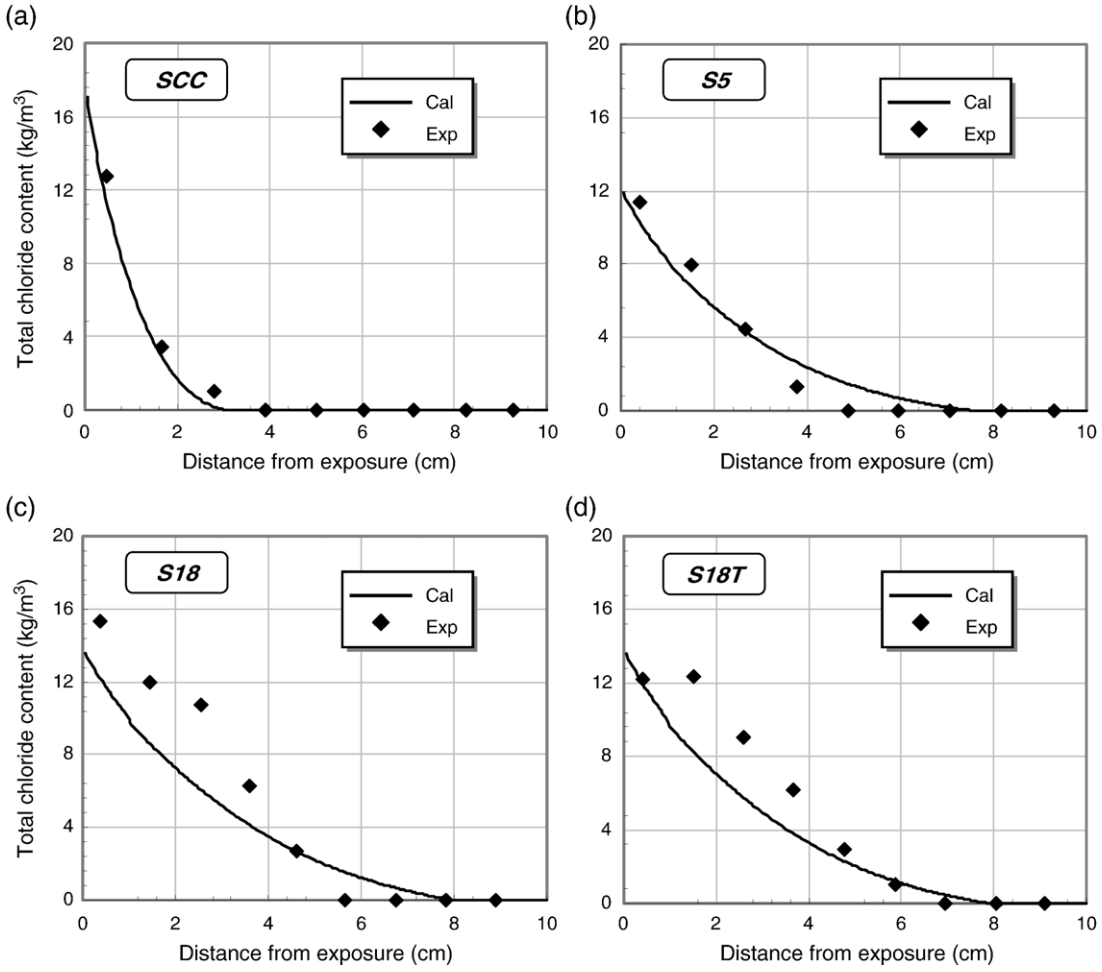

Fig. 13. Comparison of calculated and experimental results of profile of total chloride ions for concretes in Series 1.

external solution or the leachant. Then the apparent specific distribution coefficient for calcium ions was assumed to be equivalent to the following relationship;

$$\gamma^{Ca} = \frac{Q_{Esp}}{Q_{Cal}} \tag{19}$$

Where Q_{Exp} is the cumulative leaching amounts of calcium ions from diffusion leaching test (mg), Q_{Cal} is the calculated cumulative leaching amount of calcium ions (mg).

Fig. 12 provides different leaching amounts of calcium ions obtained from the diffusion leaching test and the calculation. For calculating Q_{Cal} in Eq. (19), the concentration gradient of calcium ions was maintained in Fick's law in which its concentration was constant at 0.02 mol/L. It was obvious that the amount of calcium leaching obtained from the experiments was higher than the calculation. Accordingly it was thought that the chemical potential gradient for the driving force for the calcium ions to diffuse is not expressed with the constant concentration of calcium ions in the calculation. Then the calculation results were justified using the apparent specific distribution coefficient of calcium ions as given in Eq. (19). The apparent specific distribution coefficient for calcium ions is provided in Table 5.

5.2. Initial and boundary conditions

Initial conditions are adopted for the concentration of ionic species present in the pore solution, the $Ca(OH)_2$ and C–S–H contents and the porosity which are set to be constant along with the depth ($X>0$). These values are provided in Table 5. External solution that keeps in contact with the surface of concrete under test contains only Na^+ and Cl^- with a concentration of 0.5 mol/L irrespective of time. The concentration of other ionic species in the external solution is assumed to be always zero ($t>0$).

At each particular concentration in a spatial-time discretization, the matrix of diffusion coefficients (D_{ij}) can be determined by Eq. (5). One can apply the explicit finite difference analysis to a partial differential equation as shown in Eq. (20). Hence the concentration profile of ions penetration into and/or the leaching of ions from a porous media can be achieved [35].

$$C^i_{x,t+1} = C^i_{x,t} + K_{x,t} \cdot \sum_{j=1}^{n_s} \left\{ \begin{array}{c} \gamma^i \times D_{ij,x,t} \times \left[\frac{dt}{(dx)^2}\right] \\ \times \left[C^i_{x-1,t} - 2C^i_{x,t} + C^i_{x+1,t}\right] \end{array} \right\} \tag{20}$$

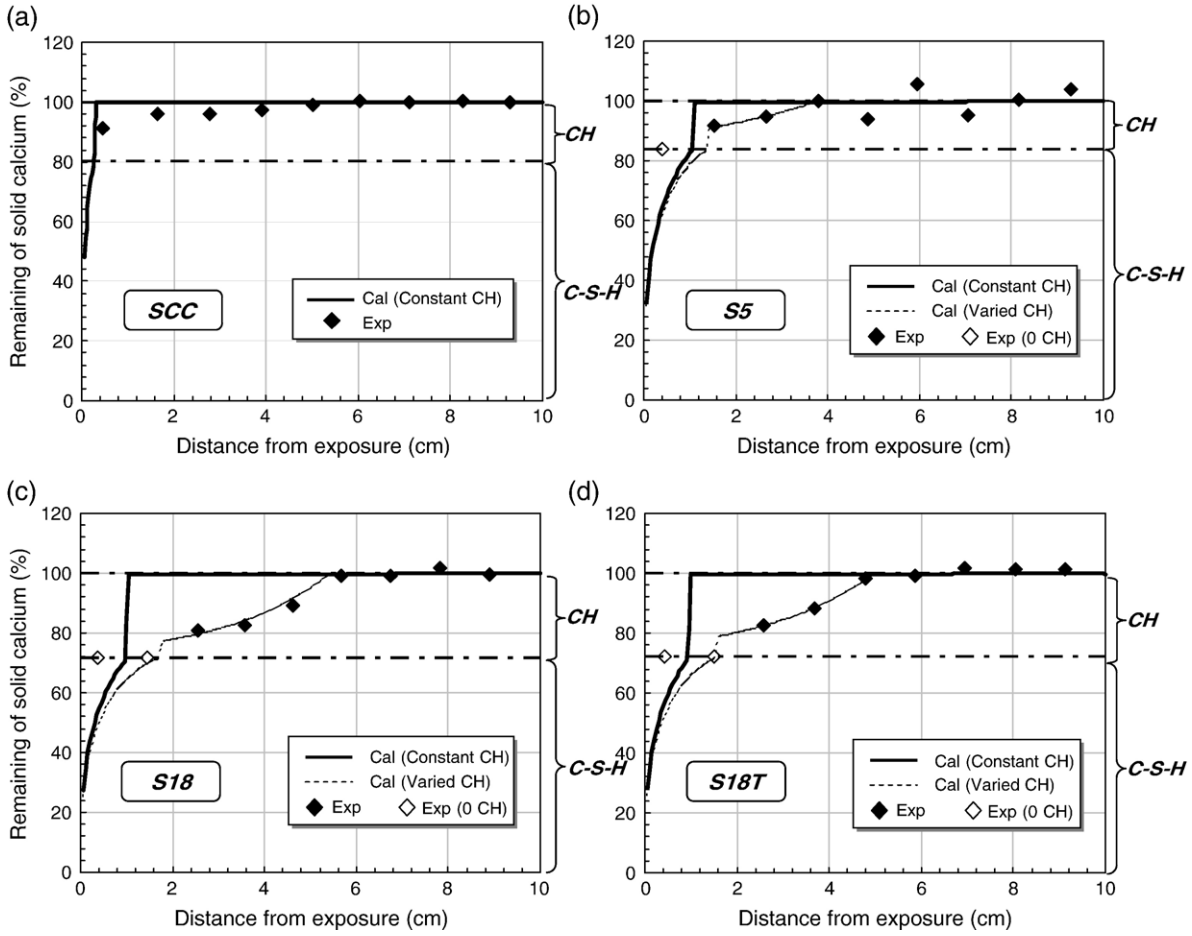

Fig. 14. Comparison of calculated and experimental results of profile of remaining calcium for concretes in Series 1.

where $C^{i}_{x,t}$ is the concentration of ionic species i in pore solution at nodal position x (cm) and nodal time t (mol/L), dt is the time discretization (s), dx is the spatial discretization (cm).

To avoid the truncating error from the approximation of the partial differential equation in Eq. (20) by using the finite difference analysis one should keep in mind that the dimensionless term in Eq. (21) should always obey the following inequality [35];

$$K_{x,t} \cdot \gamma^{i} \cdot D_{ij,x,t} \cdot \left[\frac{dt}{(dx)^2}\right] \leq 0.5 \qquad (21)$$

5.3. Verification of simultaneous ion transport model

5.3.1. Concrete in 3150 days exposure (Series 1)

Results of the numerical calculation by simultaneous ion transport model are compared with experimental results in Figs. 13 and 14 with regard to the total chloride ion profile and the profile of remaining of solid calcium in the $Ca(OH)_2$ (or CH in the figure) and C–S–H, respectively. In Fig. 14 the calcium that remained without being dissolved in the concrete is expressed by the remaining solid calcium in $Ca(OH)_2$ and C–S–H in a unit of a percentage of its initial amount. The ratio of solid calcium in $Ca(OH)_2$ and in C–S–H is based on each initial value. Since the reduction of C–S–H content was not measured experimentally, these plots of C–S–H content at the corresponding depths intentionally force to place at the initial values (blank markers) in Fig. 14.

It can be said that the results from the calculation exhibit a good agreement with the experimental results for SCC. In Fig. 13(a) of SCC specimen, the penetration depth of chloride

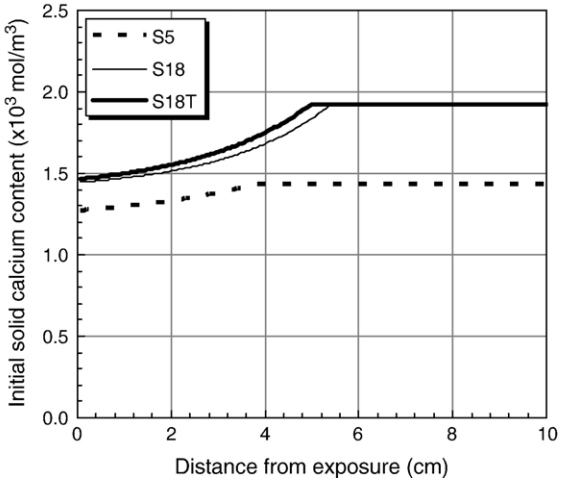

Fig. 15. Assumption of initial profile of the calcium contents of concretes in Series 1.

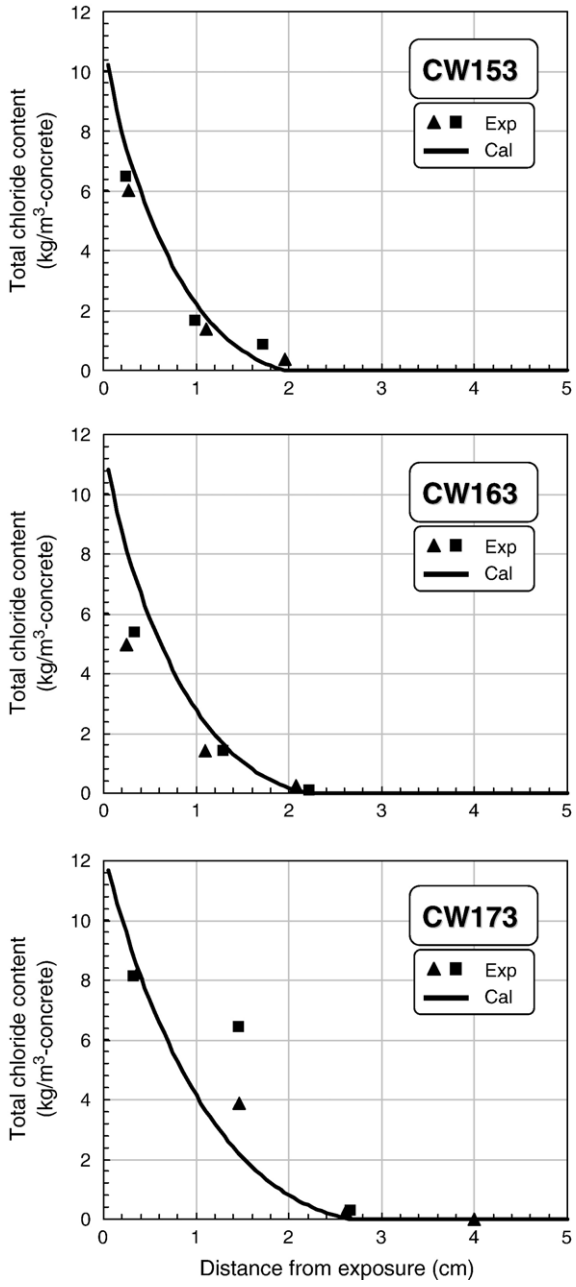

Fig. 16. Comparison of calculated and experimental results of profile of total chloride ions for concretes in Series 2.

ions is limited to 2.79 cm from the exposure surface. The lowest pore structure coefficient is largely attributed to this limited chloride penetration although low heat Portland cement used in the SCC specimen exhibited the lowest empirical chloride binding capacity. Relatively higher content of total chloride in the vicinity of its exposure surface can be noticed from the experiments and numerical calculation. Such high contents of total chloride ion near surface zone probably resulted from the highest content of the hydrated gel so as to bind relatively larger amounts of penetrating chloride ions in the SCC specimen.

It is found that the dissolution of calcium from SCC is limited to the depth less than 0.46 cm from the surface as shown in Fig. 14(a). Not only the initial amount of the hydrated cement product is relatively larger but also calcium diffusion is restricted due to the reduced pore structure coefficient. Therefore the control of the diffusion kinetics of calcium ions becomes a key factor to reduce the dissolution of calcium from the hydrated cement system.

For S5, S18 and S18T shown in Fig. 13(b) to Fig. 13(d) the calculation results tends to overestimate the depth of the chloride penetration front. In addition, the calculated total chloride contents resulted in lower than those obtained from the experiments near surface zone, especially for S18 and S18T. Linear assumption of the change in the pore structure coefficient appears to be unsuitable for these higher slump concretes. The calculation result shows that the chloride penetration is slightly reduced for S5 as compared with those for S18 and S18T.

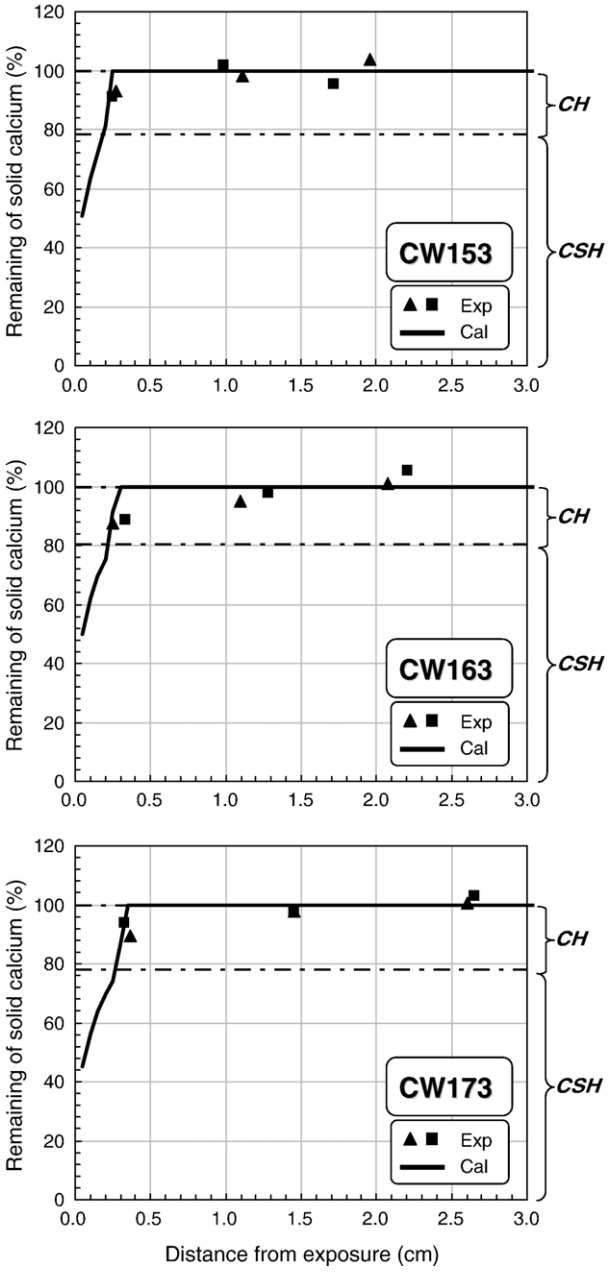

Fig. 17. Comparison of calculated and experimental results of profile of remaining calcium for concretes in Series 2.

Table 7
Input parameters for calculation by the simultaneous ion transport model (Series 2)

			CW153	CW163	CW173
Initial pore solution concentration	$[Ca^{2+}]$ (mol/L)			0.02	
	$[Na^{+}]$ (mol/L)			0.135	
	$[K^{+}]$ (mol/L)			0.104	
	$[SO_4^{2-}]$ (mol/L)			0.003	
	$[OH^{-}]$ (mol/L)			0.273	
Pore structure characteristic	Initial porosity (ε^{ini})		0.12	0.12	0.12
	Initial pore structure coefficient ε/τ^2		2.49×10^{-3}	2.66×10^{-3}	2.95×10^{-3}
Ions-solid interactions	Solid calcium	Initial $Ca(OH)_2$ ($\times10^3$ mol/m^3)	0.325	0.317	0.376
		Initial C–S–H ($\times10^3$ mol/m^3)	1.206	1.300	1.369
	Chloride binding isotherm	W_{gel} (kg/m^3–concrete)	407	435	460
		α		3.15	
		β		0.54	
	Apparent specific distribution coefficient	γ^{K}		0.77	
		γ^{Na}		0.37	
		γ^{Ca}		7.1	

Total chloride content experimentally obtained near the surface zone for S18T is lower than that of S18. Tamping would alter the physical characteristics near its surface zone. However, the penetration depth of chloride ion for S18T is similar to that for S18. Therefore, the beneficial effect by tamping is limited to only the near surface zone in terms of chloride penetration.

The dotted lines as shown in Fig. 14(b) to Fig. 14(d) are the calculation results obtained by varying initial contents of calcium with depth. Those varied calcium contents were changed from the constant calcium contents. This was because of the gradual increments of calcium at the depth ranging from 1.52 to 3.79 cm for S5, 2.54 to 5.66 cm for S18 and 2.58 to 4.78 cm for S18T, respectively, which were hardly explained by the dissolution phenomena predicted with the given solid–liquid equilibrium. Initial profiles on the calcium contents at those depths were assumed from resultant calcium profiles from TG/DTA results and are given in Fig. 15. It appears that the variation of the initial profile is larger for high slump concretes (S18 and S18T) than that of S5. Bleeding may have an influence on the varied profile of calcium in these concretes.

The calculated dissolution fronts where the content of $Ca(OH)_2$ becomes zero agree well with those obtained from the experiments. In this way, the initial profile of calcium content in concrete can be influential to simulate the dissolution front as well as the profile of the remaining calcium in the concrete. The primary reason why the dissolution front of $Ca(OH)_2$ for S18 and S18T is larger than that for S5 is because of the increased pore structure coefficient for S18 and S18T. In addition, as shown in Fig. 13 the calculated chloride penetration front for S18 and S18T is slightly deeper than that for S5 although the amount of bound chloride ion is less for S5. It is noted that the varied initial content of calcium resulted in insignificant effect on the chloride penetration behavior. It seems that chloride penetration is more influenced by the pore structure coefficient than by the amount of $Ca(OH)_2$.

5.3.2. Concrete in 420 days' exposure (Series 2)

Results of the numerical modeling by simultaneous ion transport model are compared with experimental results in Figs. 16 and 17 with regard to the total chloride ion profile and the profile of calcium remaining in the $Ca(OH)_2$ and C–S–H, respectively. Two plots of the value are drawn at each position in concrete since the chemical analysis was carried out by 2 adjacent cores for each concrete as shown in Fig. 5. Initial pore solution chemistry, the time dependent pore structure coefficients, constants α and β for the chloride binding isotherm and apparent specific distribution coefficients for concrete in Series 2 are the same as those for S18 specimen made of ordinary Portland cement. Input data for the numerical modeling is shown in Table 7. The depth-dependent effect on the pore structure coefficient is given in Fig. 18.

From Fig. 16, the numerical calculation results in similar penetration depth to those obtained from the experiments, namely 1.90 cm, 2.15 cm and 2.70 cm for CW153, CW163 and CW173, respectively. Larger penetration depth for CW173 is due to the larger pore structure coefficient although the chloride binding capacity is relatively larger than those for CW153 and CW163. Results of the migration tests to calculate the pore structure coefficients by Eq. (8) are shown in Fig. 19. It is clear that the flux of migrating chloride ion (the slope in Fig. 19) is larger for

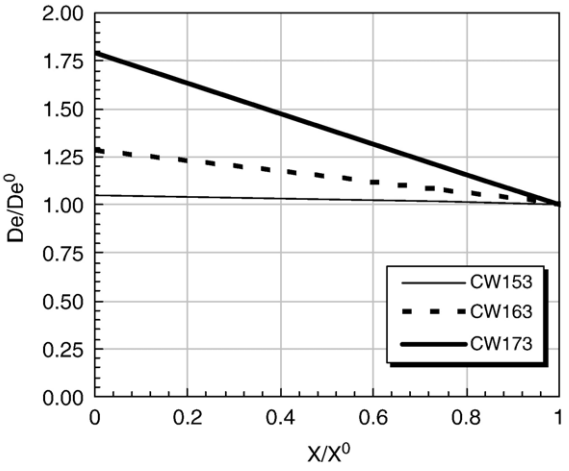

Fig. 18. Normalized position-dependent effective diffusion coefficients of concretes in Series 2.

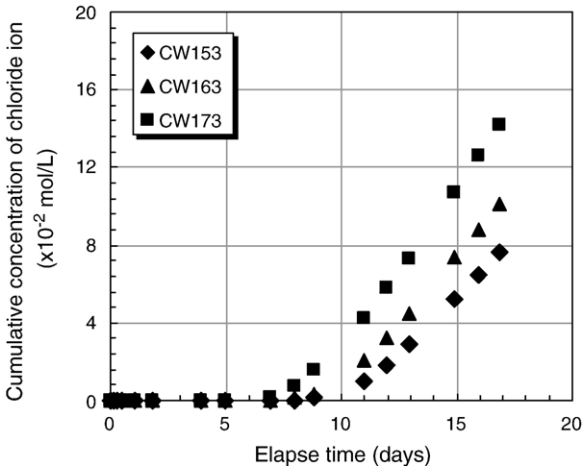

Fig. 19. Results of the steady-state migration tests of concretes in Series 2.

CW173. Calculated total chloride contents are underestimated for a depth of 1.45 cm for CW173. Uncertainty to measure the total chloride content for this concrete with larger unit water content may be involved.

From Fig. 17, the presence of $Ca(OH)_2$ crystal was experimentally identified at the nearest depth less than 0.5 cm from the exposure surface for every concrete. In other words, the dissolution front which was related to the depletion of $Ca(OH)_2$ was hardly recognized from the experiments since the interval of slice sawing from the cored concrete was 0.7 to 1.0 cm in thickness. Nevertheless to support this result the profile of the remaining solid calcium in $Ca(OH)_2$ and C–S–H is well simulated by the numerical calculation. The dissolution front of $Ca(OH)_2$ turns out to be equal to 0.15 cm, 0.20 cm and 0.25 cm for CW153, CW163 and CW173, respectively. Large dissolution front for CW173 is due to the large pore structure coefficients although the initial amount of calcium is relatively larger for CW173 than those for other concretes.

6. Conclusions

Experimental investigation and numerical modeling using simultaneous ion transport model (SiTraM) have been conducted with regard to chloride penetration and calcium dissolution on self-compacting concrete (SCC) and normal concretes. Based on this present research the following conclusions are drawn:

1. Chloride penetration test of 3150 days in continuous contact with a 0.5 mol/L NaCl solution revealed that the SCC exhibited a limited chloride penetration depth of 2.79 cm from the exposure surface. In addition, the dissolution front of $Ca(OH)_2$ was hardly recognized even at the nearest depth of 0.46 cm from the exposure surface.
2. Normal concretes with a *W/C* of 0.55 resulted in a chloride penetration depth of 4.61 cm and a dissolution front of $Ca(OH)_2$ of 1.45 cm for high slump concrete without tamping. These values were larger than those for low slump concrete of the same *W/C*. The effect of tamping for high slump concrete was limited within the near surface zone.
3. It has been proved that the Simultaneous Ion Transport Model (SiTraM) can be used for self-compacting concrete to simulate the profile of total chloride ion as well as the profile of remaining solid calcium in $Ca(OH)_2$ and C–S–H. This is partially because there is no bleeding water and hence possible defects associated with the fresh state are avoided.
4. For normal concrete with a *W/C* of 0.55, the depth-dependent pore structure coefficient and the varied initial content of calcium with the depth needed to be attentively evaluated to simulate both chloride and calcium profiles. The numerical modeling clarified that the increased pore structure coefficient had the most influential factor on both profiles as compared with the effect of the initial contents of calcium.
5. Chloride penetration test of a exposure period of 420 days confirmed that the increased unit water contents resulted in larger chloride penetration depth and larger dissolution front of $Ca(OH)_2$. The numerical calculation by the SiTraM was in general consistent with the experimental results with regards to the depth of the chloride penetration front and the profile of the remaining solid calcium in $Ca(OH)_2$ and C–S–H.

Acknowledgments

Part of this present research work was funded by the Japan Society for the Promotion of Science (Research No.: 13750438, A representative: Sugiyama Takafumi). The authors would like to thank the financial support.

References

[1] Testing and Modelling the Chloride Ingress into Concrete, in: C. Andrade, J. Kropp (Eds.), RILEM, Proceedings of the 2nd International Rilem Workshop, 2000.
[2] Sugiyama T., Ritthichauy W., Tsuji Y., Simultaneous transport of chloride and calcium ions in hydrate cement systems, Journal of Advanced Concrete Technology 1 (2) (2003) 127–138.
[3] Ritthichauy W., Sugiyama T., Tsuji Y., Calculation of diffusion coefficient of ion in multicomponent solution for ion movement in concrete, Proceedings of the Japan Concrete Institute 24 (1) (2002) 669–674.
[4] Felmy A.R., Weare J.H., Calculation of multicomponent ionic diffusion from zero to high concentration: I. The system Na–K–Ca–Mg–Cl–SO_4–H_2O at 25 °C, Geochimica et Cosmochimica Acta 55 (1991) 113–131.
[5] Felmy A.R., Weare J.H., Calculation of multicomponent ionic diffusion from zero to high concentration: II. Inclusion of associated ion species, Geochimica et Cosmochimica Acta 55 (1991) 133–144.
[6] Oelkers E.H., Physical and chemical properties of rocks and fluids for chemical mass transport calculations, in: P.C. Lichtner, C.I. Steefel, E.H. Oelkers (Eds.), Reactive Transport in Porous Media: Review in Mineralogy, The Mineralogical Society of America, Washington, DC, 1996, pp. 131–191.
[7] Newman J.S., Electrochemical Systems, Prentice-Hall, Inc, 1991.
[8] Stokes R.H., The diffusion coefficients for eight uni-univalent electrolytes in aqueous solution at 25 degree C, Contribution from the Laboratory of Physical Chemistry, 72, University of Cambridge, England, 1950, pp. 2243–2247.
[9] Mortimer R.G., Physical Chemistry, The Benjamin/Cummings Publishing Company, Inc, California, 1993.
[10] Sugiyama T., Ohata M., Igarashi T., Tsuji Y., Determination of chloride ions content in concrete by electrical migration test method, Cement Science and Concrete Technology 53 (2002) 216–223 (in Japanese).
[11] Murofushi H., Ritthichauy W., Sugiyama T., Determination of the concentration of alkali ions in pore solution of various mortars by electrochemical and natural diffusion methods, JSCE Annual Conference. Nagoya, Japan, vol. 59, 2004, pp. 11–12, (in Japanese).

[12] Sugiyama T., Shimizu S., Ritthichauy W., Tsuji Y., Determination of pore structure characteristic of mortar using a steady-state migration test, Journal of Materials, Concrete Structures and Pavements, Japan Society of Civil Engineers 64 (767) (2004) 227–238 (in Japanese).
[13] Sugiyama T., Tsuji Y., Bremner T.W., Relationship between Coulomb and migration coefficient of chloride ions for concrete in a steady-state chloride migration test, Magazine of Concrete Research 53 (01) (2001) 13–24.
[14] Andrade C., Calculation of chloride diffusion coefficients in concrete from ionic migration measurement, Cement and Concrete Research 23 (3) (1993) 724–742.
[15] Berner U.R., Evolution of pore water chemistry during degradation of cement in a radioactive waste repository environment, Waster Management 12 (1992) 201–219.
[16] Buil M., Revertegat E., Oliver J., A model of the attack of pure water or undersaturated lime solutions on cement, in: T.M. Gilliam, C.C. Wiles (Eds.), Stabilization and Solidification of Hazardous, Radioactive, and Mixed Wastes, 2nd Volume, STP 1123, ASTM, Philadelphia, 1992, pp. 227–241.
[17] Delegrave A., Gerand B., Marchand J., Modelling the calcium leaching mechanism in hydrated cement pastes, in: K.L. Scrivener, J.F. Young (Eds.), Mechanisms of Chemical Degradation of Cement-Based Systems, E&FN SPON, London, 1997, pp. 38–49.
[18] Duchesne J., Reardon E.J., Measurement and prediction of portlandite solubility in alkali solution, Cement and Concrete Research 25 (5) (1995) 1043–1053.
[19] Kobayakawa M., Ozu H., Hanehara S., The change of ion concentration in the pore solution extracted from hardened fly ash-cement mortar with curing time, Cement Science and Concrete Technology (53) (1999) 102–109 (In Japanese).
[20] Berner U.R., Modelling the incongruent dissolution of hydrated cement minerals, Radiochimica Acta 44/45 (1988) 387–393.
[21] Saito H., Tsuji Y., Kataoka H., A model for predicting degradation due to dissolution of cement hydrate, Transaction of the Japan Concrete Institute 22 (2000) 119–130.
[22] Tang L., Nilsson L.-O., Service life prediction for concrete structures under seawater by numerical approach, Proceedings of the 7th International Conference on the Durability of Building Materials and Component, E&FN Spon, Stockholm, 1996, pp. 97–106.
[23] Tang L., Nilsson L.-O., Chloride binding capacity and binding isotherms of OPC pastes and mortars, Cement and Concrete Research 23 (2) (1993) 247–253.
[24] Ushiyama H., Goto S., Diffusion of various ions in hardened portland cement paste, Proceedings of the 6th International Congress on Chemistry of Cement, Moscow 1974, vol.II-1, 1976, pp. 331–337.
[25] Goto S., Roy D.M., Diffusion of ions through hardened cement pastes, Cement and Concrete Research 11 (1981) 751–757.
[26] Ritthichauy W., Sugiyama T., Tsuji Y., Study on the influence of various inorganic salts on ion transport in cement-based material, Proceedings of the Japan Concrete Institute 26 (1) (2004) 915–920.
[27] Shigeru K., Takagi T., Goto S., Daimon M., Diffusion of ions through hardened paste of various cements, Cement Gijyutu Nenpo 37 (1983) 112–116 (in Japanese).
[28] Hanai T., Membrane and ions — theory and calculation on the transport of substances, Kagaku Dojin (1978) 154 (in Japanese).
[29] Chatterji S., Kawamura M., Electrical double layer, ion transport and reactions in hardened cement paste, Cement and Concrete Research 22 (1992) 774–782.
[30] Saito H., Nakane J., Fujiwara A., Effects of electrical potential gradients on dissolution and deterioration of cement hydrate by electrical acceleration test method, Concrete Research and Technology 4 (2) (1993) (in Japanese).
[31] Suryavanshi A.K., Swamy R.N., Influence of penetrating chlorides on the pore structure of structural concrete, Cement, Concrete, and Aggregates, CCAGDP 20 (1) (1998) 169–179.
[32] Suzuki K., Nishikawa T., Yamada Y., Taniguchi I., Analysis of hydrated phases for evaluation of the durability of concrete, Concrete research and Technology 1 (2) (1990) 39–49 (in Japanese).
[33] Taylor H.F.W., A method predicting alkali ion concentration in cement pore solutions, Advances in Cement Research 1 (1) (1987) 5–17.
[34] Sugiyama T., Hashimoto T., Tsuji Y., Hashimoto C., Application of an electrical potential technique for determining chloride diffusivity of concrete, Proceedings of the Japan Concrete Institute 19 (1) (1997) 859–864 (in Japanese).
[35] Crank J., The Mathematics of Diffusion, 2nd ed; Oxford University Press, New York, 1995.